Assessing the potential of integrating Landsat sensors for estimating chlorophyll-a concentration in a reservoir

Matias Bonansea, Claudia Rodriguez and Lucio Pinotti

ABSTRACT

Landsat satellites, 5 and 7, have significant potential for estimating several water quality parameters, but to our knowledge, there are few investigations which integrate these earlier sensors with the newest and improved mission of Landsat 8 satellite. Thus, the comparability of water quality assessing across different Landsat sensors needs to be evaluated. The main objective of this study was to assess the feasibility of integrating Landsat sensors to estimate chlorophyll-a concentration (Chl-a) in Río Tercero reservoir (Argentina). A general model to retrieve Chl-a was developed ($R^2 = 0.88$). Using observed versus predicted Chl-a values the model was validated ($R^2 = 0.89$) and applied to Landsat imagery obtaining spatial representations of Chl-a in the reservoir. Results showed that Landsat 8 can be combined with Landsat 5 and 7 to construct an empirical model to estimate water quality characteristics, such as Chl-a in a reservoir. As the number of available and upcoming sensors with open access will increase with time, we expect that this trend will certainly further promote remote sensing applications and serve as a valuable basis for a wide range of water quality assessments.

Key words | chlorophyll-a, Landsat, remote sensing, sensors, water quality

Matias Bonansea (corresponding author)
Lucio Pinotti
Instituto de Ciencias de la Tierra, Biodiversidad y Sustentabilidad Ambiental – Consejo Nacional de Investigaciones Científicas y Técnicas (ICBIA-CONICET),
Ruta Nacional 36 Km 601, Río Cuarto, Córdoba 5800,
Argentina
E-mail: *mbonansea@ayv.unrc.edu.ar*

Matias Bonansea
Claudia Rodriguez
Departamento de Estudios Básico y Agropecuarios, Facultad de Agronomía, y Veterinaria (FAyV), Universidad Nacional de Río Cuarto (UNRC),
RN36 601, Río Cuarto, Córdoba X5804BYA,
Argentina

INTRODUCTION

Monitoring water quality is a vital aspect of lake management to determine the suitability of the water for different uses (Sriwongsitanon *et al.* 2011). However, traditional monitoring programmes are time-consuming and expensive. Satellite remote sensing has the potential to complement conventional approaches to water quality monitoring. This technique offers substantial advantages over traditional monitoring methods since it provides synoptic coverage and temporal consistency of data as well as information where conventional water quality monitoring programmes are either lacking or unsatisfactory (Matthews 2011).

The Landsat program is a series of satellite missions that has been monitoring the Earth since 1972, providing the longest and the most constant satellite record of the Earth's land surface (NASA 2013). Landsat missions have contributed to the operational management and monitoring of resources for ensuring economic and environmental quality, public health and human well-being (Loveland & Dwyer 2012). The newest Landsat Data Continuity Mission (LDCM), renamed as Landsat 8, continues the Landsat program legacy (Irons *et al.* 2012). According to Loveland & Irons (2016), Landsat 8 increases the ability to detect and quantitatively characterize changes on the land surface at a scale where natural and human-induced causes of change can be detected. Although Landsat satellites, mainly 5 and 7, have significant potential for estimating several water quality parameters including water temperature (Mukherjee *et al.* 2014), water clarity (Bonansea *et al.* 2015; Olmanson *et al.* 2016), chlorophyll and phycocyanin concentrations (Wang *et al.* 2006; Tebbs *et al.* 2013), suspended sediments (Kulkarni 2011), to the best of our knowledge, there are few investigations which integrate Landsat 5 and 7 with the newest Landsat 8. Thus, the comparability of water quality assessing across different Landsat sensors

doi: 10.2166/nh.2017.116

needs to be evaluated. According to Matthews (2011), the recent launch of many new satellite instruments (e.g., Landsat 8 and Sentinel 2) is opening a new era in the remote sensing of coastal and inland waters. New sensors could improve real-time monitoring of water quality and the detection of environmental threats such as eutrophication or harmful algal blooms. Olmanson *et al.* (2016) found a strong relationship between Landsat 7 and 8 by comparing both sensors to retrieve Secchi disk transparency and coloured dissolved organic matter (CDOM). These authors also concluded that Landsat 8 seems to provide substantial improvements over earlier Landsat satellites that would open up opportunities for accurately measuring and mapping water quality characteristics from regional to global scale. Giardino *et al.* (2014) have evaluated and demonstrated the capabilities of Landsat 8, Moderate Resolution Imaging Spectroradiometer (MODIS) and RapidEye imagery for assessing chlorophyll, suspended particulate matter, CDOM and bottom depth in Lake Garda (Italy). Lymburner *et al.* (2016) demonstrated that Landsat 8 provides continuity of surface reflectance measurement enabling long-term characterization of total suspended matter dynamics for different lakes from Australia. Previous studies on water quality by remote sensing cover the entire globe with two agglomerations located in Europe and North America (Dörnhöfer & Oppelt 2016). However, few research studies have been conducted to develop appropriate assessment of water quality via remote sensing in the southern hemisphere (Dlamini *et al.* 2016).

The objective of this study was to assess the feasibility of integrating Landsat satellite 5, 7 and 8 data to estimate chlorophyll-a concentration (Chl-a) in Río Tercero reservoir (Argentina). In the province of Córdoba, surface water quality is declining and harmful and nuisance algal blooms are widespread (Amé *et al.* 2003; Mancini *et al.* 2010; Bonansea *et al.* 2016). As well, water quality information is sparse, difficult to obtain, and variable in information content and accuracy due to the fact that it has been collected by different agencies using different sampling techniques. Although the application of empirical models to estimate water quality constituents is relatively common, it is often limited to a particular sensor (Giardino *et al.* 2014). Consequently, continuity among Landsat sensors should be ensured so that long time analyses can be undertaken in lake water quality monitoring programmes. By combining Landsat 5, 7 and 8 data, we expect to generate a relevant and validated model to obtain spatial representations of Chl-a in the Río Tercero reservoir. Different studies have demonstrated that Chl-a, which is the green pigment found in almost all plants, algae and cyanobacteria, is determined by nutrient enrichment in water bodies. Furthermore, Chl-a has been recognized as one of the principal limnological parameters since it is directly related to eutrophication and trophic status of aquatic ecosystems (Moses *et al.* 2012). Therefore, an understanding of Chl-a is critical in demonstrating the extent of eutrophication and water bodies' primary productive forces (Matthews 2011).

METHODOLOGY

Study area

The Río Tercero reservoir (Figure 1) is considered the largest artificial reservoir in Córdoba province (Argentina). This reservoir, located in Calamuchita Valley, has an area of 46 km^2, a volume of 10 hm^3, a maximum and mean depth of 46.5 and 12.2 m, respectively, and an upstream catchment of 3,300 km^2. The reservoir is divided into two basins by a strait. The western basin has three branches where rivers flow and the eastern basin presents only one branch.

The Río Tercero reservoir plays an important ecological and socio-economic role in the development of cities and towns located nearby. The reservoir has multiple purposes, such as drinking water for approximately 20,000 inhabitants, power generation, flood control, irrigation, and natural habitat for wildlife. Additionally, the reservoir is located in a popular tourist and recreational area. Furthermore, since 1983, on the south shore of the lake, a nuclear power plant (CNE: 600 MWa) has been taking water from the middle section of the reservoir for cooling its nuclear reactor (Bonansea *et al.* 2015).

Field sampling

Water samples were collected on: December 9, 2006; March 20, 2009; September 07, 2010; June 15, 2015; October 12, 2015; September 01, 2016. These dates were consistent

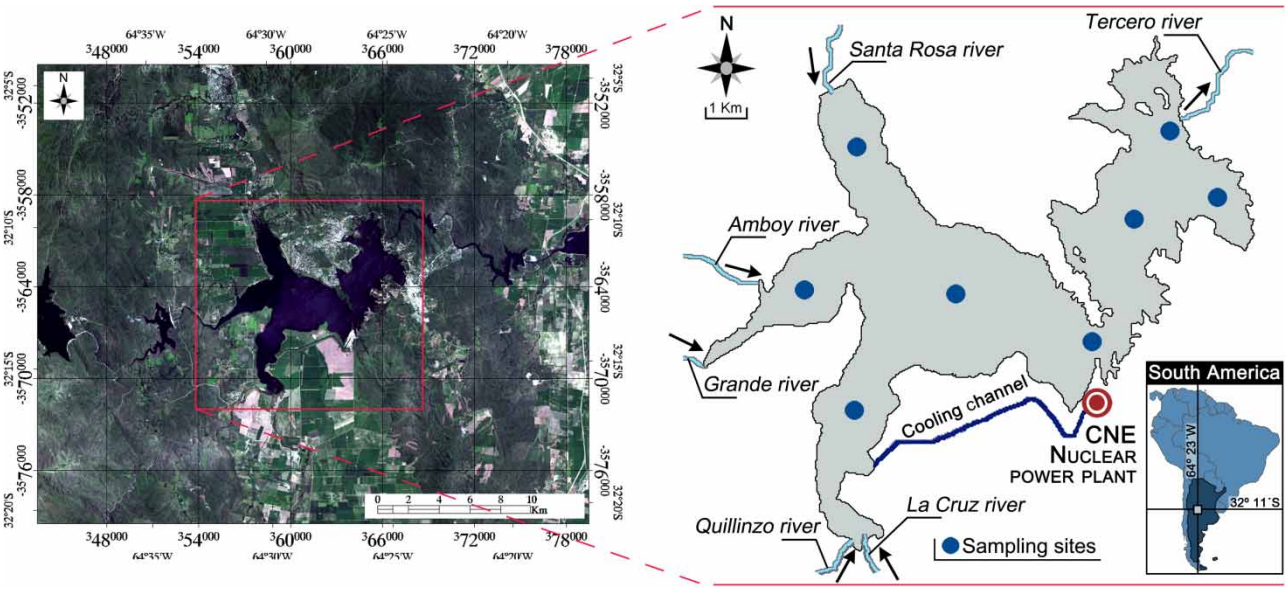

Figure 1 | Study area and position of sampling sites.

with dates of the Landsat imagery used. Eight sampling sites were surveyed, and locations for each site were recorded using a GPS device (Figure 1). After collection, Chl-a was calculated using standard analytical methods and protocols (APHA-AWWA-WEF 2000). One-litre water samples were collected at 20 cm depth. Water samples were passed through 0.45 μm pore size filters under vacuum pressure. Pigment extraction was made by manual grinding of filter papers for 1 min and soaking in acetone 90% for 10–12 h at 4.0 °C in darkness. The extracts were centrifuged (3,000 rpm, 15 min) and the concentration of Chl-a was determined by spectrophotometry using the equations of Lorenzen (1967).

Landsat imagery acquisition and processing

Estimating water quality characteristics from Landsat data requires nearly simultaneous ground observations to calibrate algorithms and minimize errors (Brezonik *et al.* 2005). Robinson (2004) suggests that field measurements and satellite overpass should be coincident in time within a period which is set by natural variation of the process being measured. In the present study, we have acquired cloud-free images Level 1 Terrain corrected (L1T) (Path: 229; Row: 82) Landsat 5 (December 09, 2006; March 20, 2009), Landsat 7 (September 07, 2010; June 17, 2015) and Landsat 8 (October 15, 2015; August 30, 2016) downloaded from the USGS Global Visualization Viewer (http://glovis.usgs.gov). We used a time window of ±3 days, defined as the difference between field measurements and satellite overpass. This time window could be useful to obtain relevant results for empirical relationships. This is because during this relatively short time frame (±3 days), water quality of Río Tercero reservoir usually does not exhibit large and rapid fluctuation. During this time window, heavy rainfall or strong winds, which could generate fluctuations in water quality conditions, were not registered in the watershed of the reservoir. As well, the selected time window is in agreement with the findings of Sriwongsitanon *et al.* (2011) and Tebbs *et al.* (2013), who suggest that this time window can be used for an empirical relationship between water quality characteristics and Landsat imagery.

Landsat 5, which provided global coverage from 1984 to 2011, was equipped with the Thematic Mapper (TM) sensor with seven spectral bands, including visible, middle- and thermal-infrared bands. Landsat 7 (launched in 1999) introduced the Enhanced Thematic Mapper Plus (ETM+), which provided multispectral coverage similar to TM but with a 60 m thermal band and a new 15 m panchromatic band (Loveland & Dwyer 2012). Since 2003, Landsat 7 has had a sensor failure called Scan Line Corrector: off (SCL-off), characterized by wedge-shaped gaps (Tebbs *et al.* 2013).

However, the radiometric and geometric performance of this sensor remains stable (Bonansea *et al.* 2015). To mitigate the impact of data gaps, a methodology adapted from the SLC Gap-Filled Products, Phase One Methodology article (USGS 2004) was used to predict the best closest value of missing pixels. Landsat 8, launched in 2013, carries two Earth observing sensors, the Operational Land Imager (OLI) and the Thermal Infrared Sensor (TIR). Improved capabilities of this satellite include an additional shorter wavelength blue band (aerosol), a narrower near-infrared band, and a 12-bit radiometric resolution against the 8 bits of previous Landsat satellites (Olmanson *et al.* 2016). The specified bandwidths and spatial resolution of the previously mentioned Landsat sensors are shown in Table 1.

To develop a sufficiently reliable relationship between water quality variables and remote sensing data, radiance transformation and atmospheric correction of satellite data must be conducted (Sriwongsitanon *et al.* 2011). The electromagnetic radiation signal collected by satellites in the solar spectrum is modified by scattering and absorption by gases and aerosols while travelling through the atmosphere from the Earth surface to the sensor (Song *et al.* 2001). Atmospheric correction to satellite data is important for rectifying the scattering and absorption effects (Sharma *et al.* 2009). Therefore, information from multitemporal data sets over regions with variable aerosol loading can be sensibly compared.

Digital numbers (DNs) of Landsat 5 and 7 were first converted to at-sensor spectral radiance (L_λ) according to Huang *et al.* (2002). DNs of Landsat 8 were converted to L_λ using the USGS Landsat 8 product instructions (USGS 2016). The Fast Line-of-sight Atmospheric Analysis of Spectral Hypercubes (FLAASH) module embedded in the Environment for Visualizing Images (ENVI) software was applied to correct images for atmospheric effects. FLAASH is an atmospheric correction tool based on MODTRAN4 (MODerate spectral resolution atmospheric TRANsmittance algorithm and computer model) (Moses *et al.* 2012).

Once atmospheric correction was complete, the normalized difference water index (NDWI) (McFeeters 1996) was used to mask out terrestrial features creating water-only images. The NDVI algorithm was used to delineate the reservoir surface on each image, while background information, such as vegetation and soil features, was restricted. The output of the NDWI algorithm ranges from -1 to 1, and the threshold value for delineating water bodies is set to ≥ 0 (McFeeters 1996). Ji *et al.* (2009) suggest that threshold adjustment in individual situations can achieve a more accurate delineation of water bodies. Thus, we set the NDWI threshold to 0.20 in order to get reliable lake surface masks. Each reservoir mask was checked by visual inspection to ensure that each land pixel in the border was removed.

Table 1 | Band specifications for Landsat sensors

	Landsat 5 TM		Landsat 7 ETM +		Landsat 8 LDCM	
Electromagnetic region	**Spatial (m)**	**Wavelength (μm)**	**Spatial (m)**	**Wavelength (μm)**	**Spatial (m)**	**Wavelength (μm)**
Aerosol					30	0.43–0.45
Blue	30	0.45–0.52	30	0.45–0.52	30	0.45–0.51
Green	30	0.52–0.60	30	0.52–0.60	30	0.53–0.59
Red	30	0.63–0.69	30	0.63–0.69	30	0.64–0.67
NIR	30	0.76–0.90	30	0.77–0.90	30	0.85–0.88
SWIR-1	30	1.55–1.75	30	1.55–1.75	30	1.57–1.65
TIR-1	120	10.40–12.50	60	10.40–12.50	100	10.60–11.19
TIR-2					100	11.50–12.51
SWIR-2	30	2.08–2.35	30	2.09–2.35	30	2.11–2.29
Pan			15	0.52–0.90	15	0.50–0.68
Cirrus					30	1.36–1.38

NIR, near infrared; SWIR, short-wave infrared; TIR, thermal infrared; Pan, panchromatic band.

Model development

Once image processing was complete, atmospherically corrected reflectance values from water-only images were used to develop relationships with measured Chl-a data. According to Matthews (2011) and Sriwongsitanon *et al.* (2011), the wavelength region of major interest to obtain information on water quality constituents is the region where water reflects and scatters most of the incoming solar radiation. This region coincides with water-leaving radiance in visible and NIR wavelengths of the electromagnetic spectrum. Thus, to facilitate comparison between Chl-a measures and imagery products, visible (blue, green and red), NIR and SWIR bands were used. In addition, based on previous research, Landsat band ratios were added to the analysis to ensure robust algorithms (Matthews 2011). Aerosol, cirrus, panchromatic and TIRS spectral bands were excluded from the analysis. Using forward step-wise multiple regression analysis ($p < 0.05$), we generated models to estimate Chl-a from Landsat imagery. These models were defined as:

$$Y_i = \beta_0 + \beta_1 X_1 + \beta_2 X_2 \ldots + \beta_v X_v + \varepsilon \quad (1)$$

where Y_i is the response of the variable Chl-a, X_n are the explanatory variables of each Landsat spectral band or band ratio, β_n are the regression coefficients, and ε is the random error.

A wide variety of candidate algorithms were tested; however, the model with the greatest adjusted R-squared value (R^2) and the lowest root mean square error (RMSE) was selected. The RMSE was defined as:

$$RMSE = \sqrt{\frac{\sum_{i=1}^{n} (X_i - X)^2}{n}} \quad (2)$$

where X_i and X are the measured and satellite-derived Chl-a, and n is the sampling size.

The prediction capability of the algorithm was validated by regression analysis. Finally, the selected algorithm was applied in Landsat imagery, producing spatial representations or thematic maps which characterized the distribution of Chl-a in the reservoir.

RESULTS AND DISCUSSION

Field data

The variation of Chl-a in the Río Tercero reservoir is shown in Table 2. Comparing sampling campaigns, ANOVA showed that Chl-a measured on June 15, 2015 and October 12, 2015 was significantly higher than the rest ($p > 0.05$). No significant differences were found between sampling sites ($p = 0.92$).

The lowest Chl-a value was measured on March 20, 2009 (1.1 μg/L), while the highest value was measured on June 15, 2015 (299.0 μg/L). In the present study, phytoplankton composition was not determined. However, high values of Chl-a observed in June and October, 2015 could be associated with *Ceratium hirundinella*. Although this widespread freshwater dinoflagellate is characteristic of temperate and subtropical lakes and reservoirs of the northern hemisphere, records of this species have increased in the southern hemisphere since 1990 when the occurrence of large *C. hirundinella* blooms became frequent (van Ginkel *et al.* 2007). During the winter of 2015, water purification plants that use Río Tercero reservoir for water supply had problems of filter clogging, taste and odours associated with this species. Therefore, to expand the application of our study, future work should be done to evaluate phytoplankton composition in the reservoir and its association with remote sensing techniques.

Regression analysis

Visible, NIR and SWIR Landsat bands and different band ratios were used for investigating the most suitable

Table 2 | Field measured Chl-a data in the Río Tercero reservoir

	Field measured Chl-a data (μg/L)	
Sampling date	**Mean ± s.d.**	**Range**
December 09, 2006	8.7 ± 3.2	2.0–12.0
March 20, 2009	13.0 ± 22.5	1.1–68.2
September 07, 2010	9.0 ± 8.4	2.1–22.8
June 15, 2015	133.9 ± 125.3	21.0–299.0
October 12, 2015	67.5 ± 38.9	16.4–122.9
September 01, 2016	12.7 ± 11.1	1.4–30.3

s.d., standard deviation.

relationship to estimate Chl-a in the Río Tercero reservoir. Table 3 shows a variety of potential regression models for Chl-a retrieval using different Landsat sensors. These models involved three or four independent variables, including different band or band ratios, with a good fit ($R^2 \sim 0.90$). Green and red bands were the most significant among all bands. Although OLI sensor has better radiometric sensitivity and signal to noise ratio, we could not prove that OLI is better than TM and ETM+ sensors. Overall, we observed that each Landsat sensor can be used to estimate Chl-a in the reservoir. The best model for TM sensor included a combination of green, red and NIR band, and the ratio green/red ($R^2 = 0.92$). A three-variable model using green and SWIR-1 bands and the ratio red/green was the best model to predict Chl-a using EMT+ sensor ($R^2 = 0.91$). The best predictive model for OLI sensor was generated using a combination of visible bands (green and red) and the ratios blue/red and green/blue ($R^2 = 0.93$).

Although we generated a different Chl-a model for each Landsat sensor, we decided to construct a new algorithm to prove that Landsat sensors can be integrated and used for water quality assessment. Thus, the best Chl-a model obtained by the combination of Landsat data was formulated as ($R^2 = 0.88$):

$$Chl\text{-a} = 110.24 - 0.68*\text{green} + 0.76*\text{red} - 129.30*\left(\frac{\text{green}}{\text{blue}}\right) - 16.62*\left(\frac{\text{NIR}}{\text{red}}\right) \quad (3)$$

where green, red, blue and NIR are the atmospherically corrected reflectance values of Landsat bands.

The 95% confidence intervals for the parameters of the model (Equation (1)) are shown in Table 4.

Figure 2 shows the comparison between predicted and observed Chl-a values. The good fit obtained from regression analysis between predicted and observed Chl-a values ($R^2 = 0.89$) and the good agreement between the gradient and intercept of the regression line indicated the high predictive capacity of the model. The RMSE of the estimated Chl-a was 18.47 μg/L producing an acceptable error associated with the estimations. This RMSE was lower than the RMSE found in other studies of Chl-a estimation by remote sensing (Dall'Olmo *et al.* 2005; Doña *et al.* 2014). The results confirmed that the methodology used for the present study is

Table 3 | Summary of regression results for various band and band ratios models to estimate Chl-a using different Landsat satellites

	Regression equation coefficients $Y = b_0 + b_1(x_1) + b_2(x_2) + b_3(x_3)$					
Independent variables	b_0	b_1	b_2	b_3	b_4	R^2
Landsat 5 TM						
Green; Red; NIR; Green/Red	15.85	−0.02	0.03	0.02	0.38	0.92
Red; NIR; Green/Red; Red/NIR	17.48	0.01	0.03	0.64	−1.30	0.91
Red; NIR; SWIR-1; Green/Blue	14.89	0.03	0.02	−0.01	5.62	0.89
Red; NIR; Green/Blue	14.79	0.03	0.02	6.08	–	0.88
Landsat 7 ETM +						
Green; SWIR-1; Red/Green	263.41	-0.25	1.24	−387.62	–	0.91
Green; SWIR-2; NIR/Red	−514.05	−0.40	−1.30	−25.37	465.70	0.91
Green; Red; Red/Green	−437.67	−1.02	1.11	485.98	–	0.90
Green; Red; Blue/Red; Green/Blue	403.08	−0.83	0.90	−56.34	−478.77	0.90
Landsat 8 OLI						
Green; Red; Blue/Red; Green/Blue	88.45	−0.48	0.50	16.83	−185.86	0.93
Green; NIR; Blue/Red; NIR/Red	−221.71	−-0.40	0.56	41.73	203.48	0.91
Green; Blue/Red; Green/Blue; Red/NIR	79.15	−0.06	15.57	−193.42	4.52	0.90
Blue/Red; Green/Blue; Red/NIR	79.63	13.60	−148.36	3.95	–	0.90

Table 4 | 95% Confidence intervals for each parameter of the used model

Parameter	Lower limit	Upper limit
β_0	93.82	126.66
β_1	−0.78	−0.57
β_2	0.61	0.92
β_3	−152.14	−106.47
β_4	−20.74	−12.50

adequate to determine Chl-a in the Río Tercero reservoir using different Landsat sensors. However, the generated algorithm is specific to the data set used in the study. Consequently, it would be necessary to obtain a greater calibration set with images acquired from different Landsat sensors and different dates to generate a multi-temporal study of Chl-a, which could improve the understanding of reservoir processes.

Mapping chlorophyll-a in the reservoir

To prove the real potential of remote sensing monitoring, the Chl-a model was applied to the Landsat imagery providing a spatial representation of Chl-a in Río Tercero during selected sampling campaigns (Figure 3). No filtering was applied to the data; however, OLI images showed a higher dynamic range than TM and ETM+ imagery. This could be related to the increase in radiometric resolution and the change in the relative spectral response of OLI sensor (Loveland & Dwyer 2012; Lymburner *et al.* 2016).

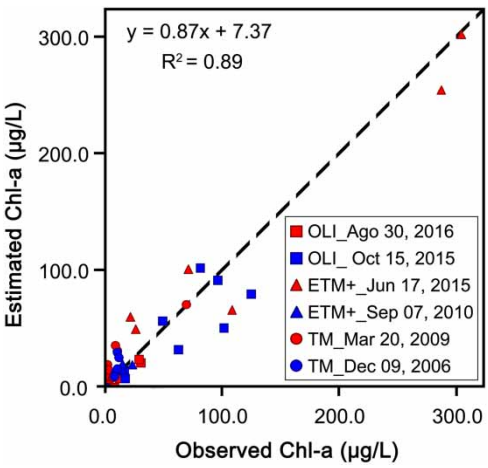

Figure 2 | Plot of estimated versus observed Chl-a with 1:1 fit line.

Satellite imagery showed that the highest values of Chl-a were recorded on June 17, 2015 coinciding with field data. Chl-a maps generated on October 15, 2015 and December 9, 2006 showed complex spatial structures of Chl-a with little surface scum areas mainly observed in the western basin of the reservoir. This could be related to river inflows. Different authors have suggested that most algal growth is located in the periphery of lakes or in areas affected by river runoff where nutrients are more concentrated (Giardino *et al.* 2010). Bonansea *et al.* (2016) demonstrated that sub-watersheds of the Río Tercero reservoir, where urban and agricultural activities are more frequent, display the highest values of nutrients loads. Over the past decades, the Río Tercero watershed has shown a continuous reduction of natural forest which, in turn, has led to an increase in human-induced activities, such as agricultural and urban residential developments. These activities have resulted in a decrease in reservoir water quality.

Matthews (2011) suggests that there are a large number of investigations that use Landsat sensors to retrieve water quality characteristics. Most of these investigations use a combination of bands and ratios, since the best model to estimate Chl-a varies from one reservoir to another. In the present study, a model to estimate Chl-a in the Río Tercero reservoir was applied using a combination of different bands (green and red) and band ratios (green/blue and NIR/red) of TM, ETM+ and OLI sensors. Similar results were obtained by Wang *et al.* (2006) and Kulkarni (2011) who demonstrated that the combination of green and red bands of TM and ETM+ Landsat sensors can be used as a strong predictor of Chl-a in different reservoirs of the United States due to the optical properties of phytoplankton. Matthews (2011) suggests that assessment of Chl-a via remote sensing uses its characteristic absorption features between 0.44 and 0.56 μm and at ~0.67 μm, which coincides with visible Landsat bands. This author also concludes that the band ratio NIR/red can be effectively exploited to determine Chl-a, as it normalizes the signal from particulate phytoplankton backscattering. In particular, Tebbs *et al.* (2013) found that the NIR/red ratio of ETM+ sensor can be used to estimate Chl-a in Lake Bogoria (Kenya). Similar results were found by Moses *et al.* (2012) using a NIR/red model applied to a

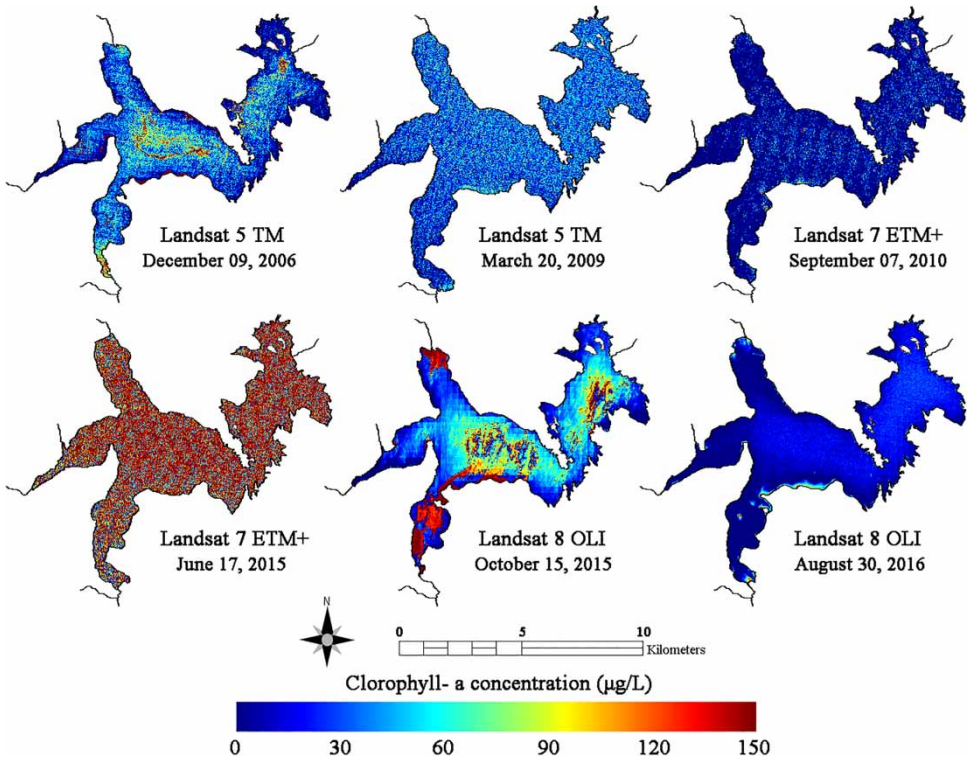

Figure 3 | Graphic representation of Chl-a distribution in the Río Tercero reservoir.

multi-temporal airborne reflectance data acquired by the hyperspectral sensor Airbone Imaging Spectrometer for Applications (AISA) in Fremont State lakes (USA). In addition, the ratio green/blue has been widely used by Östlund *et al.* (2001) with TM sensor in lakes with low Chl-a concentrations (<20 µg/L), coinciding with low Chl-a registered in Río Tercero reservoir.

The present study indicates that Landsat 8 can be combined with Landsat 5 and 7 to construct a relevant and validated empirical model for estimating water quality characteristics, such as Chl-a. Furthermore, the use of sensors with different resolutions may overcome limitations of single systems, such as the reduction to 8-day offset between the overpass of different satellites. Despite this, further research with a larger data set is needed to develop a multi-temporal study of Chl-a retrievals in the Río Tercero reservoir. A multi-temporal study would provide valuable insights into the dynamic of Chl-a over time. Thus, TM and ETM+ sensors could be used for historical measurements, while the newest OLI sensor could improve water quality assessment.

CONCLUSIONS

Water quality monitoring could benefit from spatio-temporal information derived from remote sensing data. Although TM and ETM+ sensors have significant potential to estimate several water quality characteristics, there are few investigations which integrate these sensors with the newest OLI sensor.

In the present study, we have found a strong relationship between Chl-a and different Landsat sensors. Results showed that Landsat 8 can be combined with Landsat 5 and 7 to develop an empirical model with demonstrable capability to provide accurate information of Chl-a in one of the most important multi-purpose reservoirs of Argentina. However, further research with a larger data set is needed for a multi-temporal assessment. Future research studies should include not only the assessment of Chl-a but also other water quality variables in order to understand the entire behaviour of the reservoir.

The model proposed in the present study could be used by management authorities as a valuable and reliable

measurement tool to assess water quality not only in the studied reservoir, but also in the vast numbers of lakes located at regional scale. Finally, as the number of available and upcoming open access sensors will increase with time, we expect that this trend will further promote the use of remote sensing applications as valuable sources of information for a wide range of water quality assessments.

ACKNOWLEDGEMENTS

This work was supported by CONICET and SECyT-UNRC (Secretaría de Ciencia y Técnica, UNRC). The authors would like to thank Nautical Security Direction of Córdoba province for their collaboration in sampling campaigns, and Luciana Remondino, Universidad Nacional de Río Cuarto, for her invaluable help in editing the manuscript. The anonymous reviewers are thanked for their insightful comments which helped to improve this paper.

REFERENCES

Amé, M., Diaz, M. & Wunderlin, D. 2003 Occurrence of toxic cyanobacterial blooms in San Roque reservoir (Córdoba, Argentina): a field and chemometric study. *Environmental Toxicology* **18**, 192–201.

APHA-AWWA-WEF 2000 *Standard Methods for the Examination of Water and Wastewater,* 18th edn. APHA-AWWA-WEF, Washington, DC.

Bonansea, M., Bazán, R., Ledesma, C., Rodriguez, C. & Pinotti, L. 2015 Monitoring of regional lake water clarity using Landsat imagery. *Hydrology Research* **46** (5), 661–670.

Bonansea, M., Ledesma, C. & Rodriguez, M. 2016 Assessing the impact of land use and land cover on water quality in the watershed of a reservoir. *Applied Ecology and Environmental Research* **14** (2), 447–456.

Brezonik, P., Menken, K. & Bauer, M. 2005 Landsat-based remote sensing of lake water quality characteristics, including chlorophyll and colored dissolved organic matter (CDOM). *Lake and Reservoir Management* **21** (4), 373–382.

Dall'Olmo, G., Gitelson, A., Rundquist, D., Leavitt, B., Barrow, T. & Holz, J. 2005 Assessing the potential of SeaWiFS and MODIS for estimating chlorophyll concentration in turbid productive waters using red and near-infrared bands. *Remote Sensing of Environment* **96** (2), 176–187.

Dlamini, S., Nhapi, I., Gumindoga, W., Nhiwatiwa, T. & Dube, T. 2016 Assessing the feasibility of integrating remote sensing and in-situ measurements in monitoring water quality status of Lake Chivero, Zimbabwe. *Physics and Chemistry of the Earth, Parts A/B/C* **93**, 2–11.

Doña, C., Sanchez, J., Caselles, V., Dominguez, J. & Camacho, A. 2014 Empirical relationships for monitoring water quality of lakes and reservoirs through multispectral images. *IEEE Journal of Selected Topics in Applied Earth Observations and Remote Sensing* **7** (5), 1632–1641.

Dörnhöfer, K. & Oppelt, N. 2016 Remote sensing for lake research and monitoring – Recent advances. *Ecological Indicators* **64**, 105–122.

Giardino, C., Bresciani, M., Villa, P. & Martinelli, A. 2010 Application of remote sensing in water resource management: the case study of Lake Trasimeno, Italy. *Water Resources Management* **24** (14), 3885–3899.

Giardino, C., Bresciani, M., Cazzaniga, I., Schenk, K., Rieger, P., Braga, F., Matta, E. & Brando, V. 2014 Evaluation of multi-resolution satellite sensors for assessing water quality and bottom depth of Lake Garda. *Sensors* **14** (12), 24116–24131.

Huang, C., Zhang, Z., Yang, L., Luylie, B. & Homer, C. 2002 *MRLC 2000. Image Preprocessing Procedure. USGS White Paper*. http://www.landcover.usgs.gob/pdf/image_preprocessing.pdf (accessed 29 December 2016).

Irons, J., Dwyer, J. & Barsi, J. 2012 The next Landsat satellite: the Landsat data continuity mission. *Remote Sensing of Environment* **122**, 11–21.

Ji, L., Zhang, L. & Wylie, B. 2009 Analysis of dynamic thresholds for the Normalized Difference Water Index. *Photogrammetric Engineering & Remote Sensing* **75** (11), 1307–1317.

Kulkarni, A. 2011 Water quality retrieval from Landsat TM imagery. *Procedia Computer Science* **6**, 475–480.

Lorenzen, C. 1967 Determination of chlorophyll and pheo-pigments: spectrophotometric equations. *Limnology and Oceanography* **12**, 343–346.

Loveland, T. & Dwyer, J. 2012 Landsat: building a strong future. *Remote Sensing of Environment* **122**, 22–29.

Loveland, T. & Irons, J. 2016 Landsat 8: the plans, the reality, and the legacy. *Remote Sensing of Environment* **185**, 1–6.

Lymburner, L., Botha, E., Hestir, E., Anstee, J., Sagar, S., Dekker, A. & Malthus, T. 2016 Landsat 8: providing continuity and increased precision for measuring multi-decadal time series of total suspended matter. *Remote Sensing of Environment* **185**, 108–118.

Mancini, M., Rodríguez, M., Bagnis, G., Liendo, A., Prosperi, C., Bonansea, M. & Tundisi, J. 2010 Cianobacterial bloom and animal mass mortality in a reservoir from Central Argentina. *Brazilian Journal of Biology* **70**, 841–845.

Matthews, M. 2011 A current review of empirical procedures of remote sensing in inland and near-coastal transitional waters. *International Journal of Remote Sensing* **32** (21), 6855–6899.

McFeeters, S. 1996 The use of normalized difference water index (NDWI) in the delineation of open water features. *International Journal of Remote Sensing* **17**, 1425–1432.

Moses, W., Gitelson, A., Perk, R., Gurlin, D., Rundquist, D., Leavitt, B., Barrow, T. & Brakhage, P. 2012 Estimation of chlorophyll-a

concentration in turbid productive waters using airborne hyperspectral data. *Water Research* **46** (4), 993–1004.

Mukherjee, S., Joshi, P. & Garg, R. 2014 A comparison of different regression models for downscaling Landsat and MODIS land surface temperature images over heterogeneous landscape. *Advances in Space Research* **54** (4), 655–669.

NASA 2013 *Program-Level Requirements on the Landsat Data Continuity Mission Project: Appendix N to the Earth Systematic Mission Program Plan*. Washington, DC, 20 pp.

Olmanson, L., Brezonik, P., Finlay, J. & Bauer, M. 2016 Comparison of Landsat 8 and Landsat 7 for regional measurements of CDOM and water clarity in lakes. *Remote Sensing of Environment* **185**, 119–128.

Östlund, C., Flink, P., Strömbeck, N., Pierson, D. & Lindell, T. 2001 Mapping of the water quality of Lake Erken, Sweden, from imaging spectrometry and Landsat Thematic Mapper. *Science of the Total Environment* **268** (1), 139–154.

Robinson, I. 2004 *Measuring the Oceans From Space: The Principles and Methods of Satellite Oceanography*. Springer Science & Business Media, UK.

Sharma, A., Badarinath, K. & Roy, P. 2009 Comparison of ground reflectance measurement with satellite derived atmospherically corrected reflectance: a case study over semi-arid landscape. *Advances in Space Research* **43** (1), 56–64.

Song, C., Woodcock, C., Seto, K., Lenney, M. & Macomber, S. 2001 Classification and change detection using Landsat TM data: when and how to correct atmospheric effects? *Remote Sensing of Environment* **75** (2), 230–244.

Sriwongsitanon, N., Surakit, K. & Thianpopirug, S. 2011 Influence of atmospheric correction and number of sampling points on the accuracy of water clarity assessment using remote sensing application. *Journal of Hydrology* **401** (3–4), 203–220.

Tebbs, E., Remedios, J. & Harper, D. 2013 Remote sensing of chlorophyll-a as a measure of cyanobacterial biomass in Lake Bogoria, a hypertrophic, saline–alkaline, flamingo lake, using Landsat ETM + . *Remote Sensing of Environment* **135**, 92–106.

USGS 2004 *Phase 2 Gap-Fill Algorithm: SLC-off Gap-Filled Products Gap-Fill Algorithm Methodology*. http://landsat.usgs.gov/documents/L7SLCGapFilledMethod.pdf (accessed 29 December 2016).

USGS 2016 *Landsat 8 Data Users Handbook*. https://landsat.usgs.gov/sites/default/files/documents/Landsat8DataUsersHandbook.pdf (accessed 29 December 2016).

Van Ginkel, C., Cao, H., Recknagel, F. & Du Plessis, S. 2007 Forecasting of dinoflagellate blooms in warm-monomictic hypertrophic reservoirs in South Africa by means of rule-based agents. *Water SA* **33** (4), 531–538.

Wang, F., Han, L., Kung, H. & Van Arsdale, R. 2006 Applications of landsat5 TM imagery in assessing and mapping water quality in Reelfoot Lake, Tennessee. *International Journal of Remote Sensing* **27** (23), 5269–5283.

First received 23 June 2017; accepted in revised form 2 December 2017. Available online 18 December 2017